Macromolecules

Article

pubs.acs.org/Macromolecules

# Perfectly Ordered Patterns via Corner-Induced Heterogeneous Nucleation of Self-Assembling Block Copolymers Confined in Hexagonal Potential Wells

Hanlin Deng,[†] Nan Xie,[†] Weihua Li,*[,†] Feng Qiu,[†] and An-Chang Shi[‡]

[†]State Key Laboratory of Molecular Engineering of Polymers, Collaborative Innovation Center of Polymers and Polymer Composite Materials, Department of Macromolecular Science, Fudan University, Shanghai 200433, China

[‡]Department of Physics and Astronomy, McMaster University, Hamilton, Ontario Canada L8S 4M1

Supporting Information

**ABSTRACT:** The ordering dynamics of cylinder-forming diblock copolymer/homopolymer blends confined in hexagonal potential wells is systematically investigated using time-dependent Ginzburg–Landau (TDGL) theory. It is demonstrated that a high-efficient method to obtain large-scale ordered hexagonal patterns is to utilize corner-induced heterogeneous nucleation processes, in which nucleation events with controlled positions and orientations are triggered exclusively at the six corners of the confining hexagonal wells. Subsequent growth of the six domains originated from the corners leads to the formation of perfectly ordered patterns occupying the entire hexagonal well. The heterogeneous nucleation rate is regulated by the homopolymer concentration as well as the surface potential of the confining walls. Defect-free hexagonal patterns are obtained in hexagons with a diagonal size containing up to 61 cylinders (about 2 $\mu$m). The robustness of the method is examined by studying the tolerance window of the size-commensurability of the confining wells. The results indicate that controlled heterogeneous nucleation provides an efficient method for the fabrication of large-scale ordered patterns using graphoepitaxy of block copolymer self-assembly.

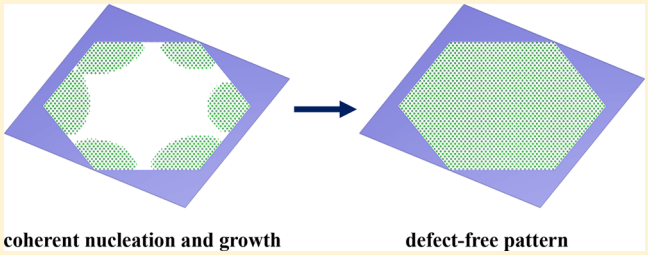


## INTRODUCTION

Since the 1970s the development of semiconductor industry has been following the famous Moore's law,[1,2] thus demanding the manufacturing of devices with smaller nanometer-scale structures which in general requires higher cost. In both scientific and technological communities, many efforts have been devoted to exploration of alternative patterning techniques to replace or improve the conventional lithography techniques. Among many different proposals, directed self-assembly (DSA) of block copolymers has been intensively studied and has been regarded as one of the most appealing new-generation lithography techniques.[3−7] The DSA of block copolymers is a bottom-up patterning technique combining the advantages of traditional lithographic techniques and the self-assembling ability of block copolymers on the length scale of 5−100 nm, thus providing a patterning technology with high-resolution and high-throughput at a low cost. One of the primary tasks of DSA is to yield large-scale ordered, and geometrically simple, patterns, i.e., cylinders (dots)[8−11] or lamellaes (stripes),[12−18] for both fundamental research interest and practical application in the fabrication of high-density storage media and other devices. Two types of DSA techniques, chemical epitaxy[8−13,15,17] and graphoepitaxy,[19−26] have been proposed. Moreover, these two DSA techniques have also been used to fabricate some device-oriented irregular structures which have potential applications in the manufacture of integrated circuits.[27−29]

One of the most concerned issues in DSA is the directing efficiency which directly determines the manufacturing cost. The directing efficiency can be quantified by the density multiplication (DM), which is defined as the density ratio of the directed block copolymer domains to the prefabricated directing patterns. In general, there is an upper limit of the directing efficiency in the DSA using chemical epitaxy or graphoepitaxy.[8,15,17] Specifically, in the DSA using graphoepitaxy for large-scale ordered cylinder patterns, where the directing geometrical pattern is composed of hexagonal array of sparsely spaced nanoposts, an obvious limit of DM, smaller than 25, was recorded in experiments.[8] The presence of this efficiency limit can be attributed to the characteristics of the dislocation pairs, as demonstrated in the dynamic simulations of time-dependent Ginzburg–Landau (TDGL) theory.[9,10] In addition, the TDGL simulations reveal that the underlying mechanism for the presence of the limit of directing efficiency is the spontaneous ordering of the system via spontaneous nucleation or spinodal kinetics.

**Received:** April 1, 2015
**Revised:** May 29, 2015
**Published:** June 12, 2015





DOI: 10.1021/acs.macromol.5b00681
*Macromolecules* 2015, 48, 4174−4182

An effective method to enhance the directing efficiency is to regulate the thermodynamics of the system, such that the phase separation kinetics is dictated by a controlled nucleation process, instead of the spontaneous spinodal kinetics. In general, any metastable phase has the tendency to transform into more stable phases via nucleation processes driven by thermal fluctuations. In block copolymers, a metastable disordered phase would transform into a more stable ordered phase via a nucleation and growth mechanism. Lamellar[30,31] and cylinder domains[32−34] nucleated from a disordered state have been observed in experiments and simulations. On the basis of a series of simulations of DSA of block copolymers, we have proposed a successful strategy for the fabrication of large-scale ordered patterns via the heterogeneous nucleation process induced by a periodic array of anisotropic nucleation agents.[34]

Although the strategy proposed by Xie et al.[34] can lead to large-scale ordered patterns, two aspects of that specific proposal can be improved. First of all, it was proposed to use two circular potential wells to control the orientation of nucleated domains. Although this is a valid method, the distance between the double potential wells was taken as same as the domain spacing of block copolymers. Therefore, it prevents this method from reaching a much finer size level. Second, there exists a wavy fluctuation of domain alignment, which becomes severe for sparsely spaced nucleation agents. A large position fluctuation will lead to defects at the boundaries between neighboring domain grains. In order to overcome these shortcomings of this proposed design of the directing field, it is desirable to improve the design of nucleation agents and the directing fields. In this paper, we demonstrated that a directing field in the form of a hexagonal potential well can act as nucleation agents with controlled position and orientation, as well as directing field for the growth of the nucleated domains.

The proposed directing design of a hexagonal potential well can be considered as a confining environment for block copolymers, which is able to not only lead to novel structures but also improve the order of morphologies.[35−42] One of the most successful examples is the implementation of a *lateral confinement* in the form of hexagons on the fabrication of perfectly ordered hexagonally packed cylindrical patterns by Xu et al.[43] In this experiment, nearly defect-free hexagonal patterns have been obtained in the hexagonal confinement with sizes up to 1175 nm, demonstrating a valid directing effect of the hexagonal confinement. However, it has been shown that when the diagonal size of hexagons becomes larger than 1300 nm, a noticeable amount of defects are observed. The formation of defects in a large hexagon is attributed to the spontaneous nucleation processes in the system. From these observations it can be concluded that if the spontaneous or homogeneous nucleation events were suppressed and, at the same time, controlled nucleation events were introduced into the hexagonally confined system, the directing efficiency of the geometry could be enhanced significantly. From classical nucleation theory, it is well-known that edges and corners of a confining system can act as heterogeneous nucleation sites with different nucleation rate. A simple application of the classical nucleation theory to the confining hexagons produces that, for a set of appropriate interaction parameters, the edges and the corners of hexagons can act as nucleation agents. The corners have the lowest nucleation barrier, and thus could act as primary nucleation sites for the ordering of the system. Furthermore, the six sidewalls have equal ability to induce nucleation events (details of the classical nucleation theory calculation are given in the Supporting Information, or SI). On the other hand, the walls of hexagons could also induce nucleations with a higher energy barrier. The positions of the domains originated from these nucleation events are not well controlled. The nucleation rate at the six corners is higher than that at the six sides because each corner is the joint of two sides with a fixed angle of 120 deg, and thus there is a large energy gain due to the interaction with the edges (see SI). From these considerations, a design for valid directing fields is in the form of a hexagon.

The model system of choice in our study is thin films of AB diblock copolymers and C homopolymers confined in a hexagonal potential well with neutral top and bottom surfaces. The block copolymers form an ordered phase of hexagonally packed cylinders in bulk, whereas a small amount of C homopolymers is added to the blends to regulate the phase behavior of the blend. In particular, the homopolymer concentration is used to control the homogeneous nucleation rate of the cylindrical phase from a metastable disordered phase. Note that a lot of 3D structures differing from the hexagonal cylinders become thermodynamically stable in the hexagonal confinement, however, the cylindrical morphology is always the stable structure when the size of hexagons is large and commensurate to the domain period. This is why the hexagonally lateral confinement is able to generate ordered hexagonal cylinders except for the presence of defects in extremely large hexagons.[43]

The ordering kinetics of the AB/C blend is studied using TDGL simulations, focusing on the mechanism of corner-induced heterogeneous nucleation events in the confining hexagons. As nucleation only occurs at the vicinity of order−disorder transition when thermal fluctuations are suppressed (e.g., increasing molecular weight), the TDGL theory which is valid for weakly segregated system is suitable to describe the considered AB/C blend. Furthermore, the TDGL simulation, as a high-efficient method, has been proven to be a useful tool for the study of nucleation processes which usually requires a macroscopic size of samples.[32−34,44,45]

## THEORY AND METHODS

We consider a blend of AB-diblock copolymer and C-homopolymer (AB/C) which is vertically confined between two parallel neutral surfaces in $z$ direction and laterally confined in a hexagonal well with diagonal length of $D$ in $xy$ plane. This AB/C blend is characterized by the composition of C-homopolymer, $\bar{\phi}_C$, together with the block ratio of the A-block in the AB-diblock copolymer, $f$. Two independent order parameters are chosen to describe the phase separation of the three-component system, i.e., two density differences, $\phi(\mathbf{r})=\phi_A(\mathbf{r})-\phi_B(\mathbf{r})$ and $\eta(\mathbf{r})=\phi_A(\mathbf{r})+\phi_B(\mathbf{r})-\psi_C$, where $\phi_K(\mathbf{r})$(K=A, B, and C) denotes the local density of K species at a given position $\mathbf{r}$. The free energy as a functional of the spatial functions of the two order parameters, which can be used to qualitatively describe the phase behavior of the AB/C blend, has been proposed by Ohta and Ito[46,47] based on the Ohta-Kawasaki model,[48−50]

$$F[\phi, \eta] = F_S[\phi, \eta] + F_L[\phi, \eta] + \int \mathrm{d}\mathbf{r}\, H_{ext}(\mathbf{r})\phi(\mathbf{r}) \quad (1)$$

where $F_S$ is the short-range interaction term which originates from the well-known Ginzburg−Landau free energy and is composed of interfacial energy and local interaction energy, and it can be expressed as



DOI: 10.1021/acs.macromol.5b00681
*Macromolecules* 2015, 48, 4174−4182

$$F_S[\phi, \eta] = \int d\mathbf{r} \left\{ \frac{D_1[\nabla\phi(\mathbf{r})]^2}{2} + \frac{D_2[\nabla\eta(\mathbf{r})]^2}{2} + f_\phi[\phi] + f_\eta[\eta] + f_{int}[\phi, \eta] \right\} \quad (2)$$

Here $D_1$ and $D_2$ are two positive constants related to the interfacial properties between A and B components and between AB-diblock copolymer and C-homopolymer. The immiscibility degrees between A and B components, and between AB-diblock copolymer and C-homopolymer, are included into the two energy terms $f_\phi[\phi]$ and $f_\eta[\eta]$, respectively, which can be simply expressed by their derivatives $df_\phi/d\phi = -A_\phi \tanh \phi + \phi$ and $df_\eta/d\eta = -A_\eta \tanh \eta + \eta$. The two parameters $A_\phi$ and $A_\eta$ are required to be greater than one to drive the microphase or macrophase separation. A number of intercrossing terms of the two order parameters are introduced to describe the interaction energy between the three components, and they are given by $f_{int} = b_1\eta\phi - b_2\eta\phi^2/2 - b_3(\eta\phi^3 + \eta^2\phi + \eta^3\phi) + b_4\eta^2\phi^2/2$. Although the derivation is rather phenomenological, these coefficients $b_1$, $b_2$, $b_3$, and $b_4$ have explicit physical meanings.[46,47]

The contribution of the connectivity between the A- and B-blocks to the free energy is not included in the short-range terms, and it cannot be accounted for by any local energy term because of the chain-like behavior of polymers. In recent decades, the self-consistent field theory (SCFT) has been developed to compute the free energy of the Gaussian-chain polymers accurately in the level of mean-field approximations.[51,52] It is possible to develop a dynamics theory based on SCFT.[53] However, the free energy functional of SCFT is not explicit, thus limiting its application in the study of dynamics. Fortunately, a simple and validated free-energy functional for AB diblock copolymers was proposed early in 1986 by Ohta and Kawasaki.[54] The availability of the Ohta-Kawasaki free energy functional has enabled the application of TDGL simulations in the study of the phase separation dynamics in block copolymers. Subsequently, Ohta and Ito extended the free energy functional from the simple AB diblock copolymers to AB/C blends.[46] The long-range term, $F_L$, can be written as,

$$F_L[\phi, \eta] = \int d\mathbf{r} \int d\mathbf{r}' \, G(\mathbf{r}, \mathbf{r}') \left[ \frac{\alpha\delta\phi(\mathbf{r})\delta\phi(\mathbf{r}')}{2} + \beta\delta\phi(\mathbf{r})\delta\eta(\mathbf{r}') + \frac{\gamma\delta\eta(\mathbf{r})\delta\eta(\mathbf{r}')}{2} \right] \quad (3)$$

where $\delta\phi(\mathbf{r}) = \phi(\mathbf{r}) - \bar{\phi}$, $\delta\eta(\mathbf{r}) = \eta(\mathbf{r}) - \bar{\eta}$ , and $\bar{\phi}$, $\bar{\eta}$ represent the full spatial average of the two parameters, respectively. The coefficients $\alpha$, $\beta$ and $\gamma$ satisfy the relation of $\beta^2 = \alpha\gamma$ and they are related to the polymerization degrees of AB and C.[46] In the above expression, the Green Function of $G(\mathbf{r}, \mathbf{r}')$, with a Coulomb interaction form, characterizes the long-range feature of the chain connectivity of the diblock copolymer.

Since we consider the AB/C blend laterally confined in the hexagonal well, we introduce an external potential field, $H_{ext}(\mathbf{r})$, to model the preferential interactions of the sidewalls. Similar to our previous work,[9,10,34] the free-energy contribution from the external field is expressed as $\int d\mathbf{r}\, H_{ext}(\mathbf{r})\phi(\mathbf{r})$, where the form of the external field is chosen as

$$H_{ext}(\mathbf{r}) = -\frac{1}{2}\Lambda_0\{\tanh[(\sigma - d(\mathbf{r}))/\varepsilon] + 1\} \quad (4)$$

where the shortest distance of the position $\mathbf{r}$ to any sidewall of the hexagonal well is $d(\mathbf{r}) < 2\sigma$. The field strength, the interaction distance, and the potential steepness are denoted as $\Lambda_0$, $2\sigma$, and $\varepsilon$, respectively.

With the given free-energy functional in eq 2, the phase separation dynamics of the AB/C blend is described by two conserved Cahn–Hilliard dynamic equations

$$\frac{\partial\phi}{\partial t} = M_1\nabla^2\frac{\delta F[\phi, \eta]}{\delta\phi} + \xi_\phi(\mathbf{r}, t)$$
$$\frac{\partial\eta}{\partial t} = M_2\nabla^2\frac{\delta F[\phi, \eta]}{\delta\eta} + \xi_\eta(\mathbf{r}, t) \quad (5)$$

where $M_1$ and $M_2$ are two mobility coefficients, and $\xi_\phi$ and $\xi_\eta$ are the random noise terms, which satisfy the fluctuation dissipation theorem.

Similar to our previous work, we choose the relevant parameters as $f = 0.40$, $D_1 = 0.5$, $D_2 = 1.0$, $M_1 = M_2 = 1.0$, $A_\phi = 1.260$, $A_\eta = 1.100$, $b_1 = -0.05$, $b_2 = 0.05$, $b_3 = 0.01$, $b_4 = 0.10$, $\psi_C = 0.20$, $\sigma = 0.15L_0$, and $\varepsilon = 0.50L_0$, where $L_0$ is the cylinder-to-cylinder distance of the AB/C blend, and it varies with $\bar{\phi}_C$. First, we will regulate the heterogeneous nucleation process by tuning the two variables, the concentration of the C-homopolymer $\bar{\phi}_C$ and the field strength $\Lambda_0$, to yield prior nucleation events exclusively at the six corners and thus to achieve perfectly ordered hexagonal patterns. Then we investigate the tolerance of the domain growth to the incommensurate degree between the hexagonal size and $L_0$ with optimized $\bar{\phi}_C$ and $\Lambda_0$ by varying the diagonal length of hexagons, $D = m\,L_0$. In order to simulate the samples as large as possible, we reduce our simulation to be two-dimensional under the assumption that perpendicularly standing cylinders are formed in the thin films with neutral top and bottom surfaces unless otherwise specified. A discretization scheme of cell dynamic simulations (CDS) similar to that in our previous work is employed to integrate the TDGL equations.[34]

## RESULTS AND DISCUSSION

For the AB/C blends confined in a hexagonal well, it is observed that the kinetic behavior is mainly controlled by three parameters: the average C-homopolymer concentration $\bar{\phi}_C$, the sidewall-polymer interaction parameter $\Lambda_0$, and the size of the hexagon $mL_0$ where $L_0$ is the bulk domain spacing between the cylinders. The influence of the C-homopolymer concentration on the phase separation kinetics of the AB/C blend in bulk has been studied previously,[34] indicating that the phase separation kinetics varies from spinodal kinetics to nucleation and growth as $\bar{\phi}_C$ is decreased, and the nucleation rate, defined as the probability of one nucleation event occurred in a unit volume per unit time, is continuously reduced until the disordered phase becomes thermodynamically stable.

In the geometrically confined system, the introduction of sidewalls changes the nucleation conditions near the geometrical boundaries. Specifically, for a nucleus in contact with the sidewall, a portion of the interface between the disordered domain and the ordered domain becomes an interface between the ordered domain and the sidewall (Figure S4, Supporting Information). This change results in a different (lower) energy barrier of nucleation at the sidewalls or at the corners from (than) the homogeneous nucleation barrier. Thus, heterogeneous nucleation processes become important events in the confined system. A calculation based on the classical nucleation theory indicates that the free energy barrier can be lowered by the surface potential of the sidewalls (Figure S5), but the critical size of nucleus is unchanged in the heterogeneous nucleation (eqs S3 and S12). As a consequence, the heterogeneous nucleation rate at the corners is modified to be significantly higher than the spontaneous one as well as that at the sidewalls. Therefore, the corners of the confined hexagonal well can act as the nucleation agents to induce ordered domains with prescribed positions and orientations. The growth and merge of those coherent domains leads to the formation of large-scale ordered patterns.

**Effect of Homopolymer Concentration.** In this subsection we examine the effects of varying the homopolymers



DOI: 10.1021/acs.macromol.5b00681
Macromolecules 2015, 48, 4174−4182

concentration, $\bar{\phi}_C$, on the ordering process of morphologies self-assembled in the AB/C blend confined in the hexagonal wells. Typical morphologies with a given size $D = 41.00\ L_0$ of the hexagons and potential strength $\Lambda_0 = 0.0020$ for three different homopolymer concentrations, $\bar{\phi}_C = 0.100$, 0.050, and 0.035, are presented in Figure 1. For each sample, the

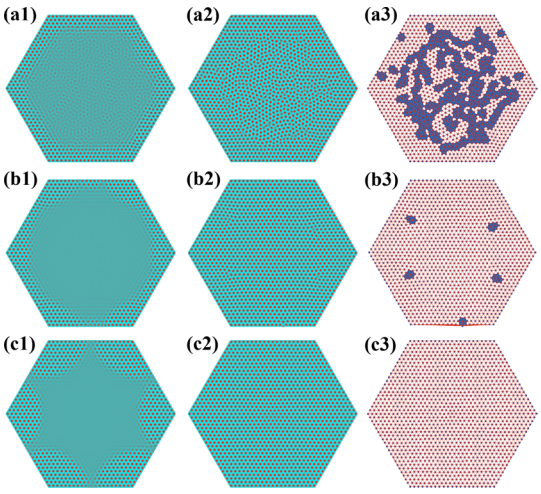


**Figure 1.** Morphologies (left and middle columns) at two typical time steps and corresponding Delaunay triangular plots (right column) at the moment when the phase separation expands the entire hexagonal sample. The diagonal size and field strength are fixed as $D = 41.00\ L_0$ and 0.0020, respectively. From top to bottom, homopolymer concentrations, $\bar{\phi}_C$, are 0.100, 0.050, and 0.035, respectively. (a1 and a2) $t = 4 \times 10^4$ and $6 \times 10^4$. (b1 and b2) $t = 9 \times 10^4$ and $24 \times 10^4$. (c1 and c2) $t = 18 \times 10^4$ and $34 \times 10^4$.

morphologies at two stages, early and late, in the phase separation processes are shown. At the early stage, the phase separation starts at the sides and corners of the hexagonal well, whereas at the late stage, the self-assembled domains grow and merge to occupy the entire hexagonal well. It is noticed that the cylinder-to-cylinder distance $L_0$ slightly depends on $\bar{\phi}_C$, and thus it is determined individually for each value of $\bar{\phi}_C$. In order to examine the ordering process quantitatively, we calculate the number of defects, i.e., the sites with number of nearest neighbors not equal to six. Specifically the defects are identified by the Delaunay triangular algorithm.[9] The corresponding Delaunay triangular plots are given for the three morphologies in Figure 1. Consequently, the defect concentrations, defined as $f_{DF} = n_{DF}/n_{MD} \times 100\%$ where $n_{DF}$ and $n_{MD}$ are the total numbers of defects and microdomains, respectively, are determined as 18.65%, 0.70%, and 0 for the three samples of $\bar{\phi}_C = 0.100$, 0.050, and 0.035 at the late stage, respectively.

Apparently, for $\bar{\phi}_C = 0.100$, the phase separation kinetics is characterized by the occurrence of spontaneous nucleation events in the system. However, it is interesting to notice that the spontaneous nucleation differs from the multiple homogeneous nucleation events in the bulk. In particular the spontaneous nucleation in the current system exhibits a two-stage behavior (Figure 1a). At the initial stage right after quenching, surface wetting of the sidewalls induces large composition fluctuations and therefore triggers phase separations near the sidewalls immediately.[55] Then these surface-induced nucleation domains grow by expanding away from the sidewalls. The first stage of the domain growth continues until a spontaneous phase separation occurs in the central area after a short incubation time, at which random fluctuations result in homogeneous nucleation events in the central region of the sample.[32,34] As a consequence, there is a remarkable difference in the domain order between the two regions, i.e., near the sidewalls and in the central area, because of the two distinct mechanisms of ordering processes in the two stages. Near the sidewalls, the domains are formed via surface-induced nucleation. Although the precise positions of the nuclei induced by the sidewalls are not well controlled, their orientation is directed by the orientation of the sidewalls. As such, the growth of the ordered domains leads to better ordered structures. On the other hand, the lack of positional control of the side-induced nucleation events results in mismatched boundaries between the growing domains from the sidewalls, thus the formation of a small amount of defects. In contrast, the central domains are formed via spontaneous nucleation events, thus either their positions or orientations are not coherent, resulting in structures with a high density of defects. The overall defect concentration is as high as $f_{DF} \approx 18.65\%$ in this case. It is expected that the initial high concentration of defects can be reduced by subsequent annealing process, but it usually takes an extremely long time to remove all of defects.[41]

When the homopolymer concentration is decreased to $\bar{\phi}_C = 0.050$, the morphology shown in Figure 1b clearly indicates that the system exhibits a different kinetic behavior as compared with the case of $\bar{\phi}_C = 0.100$. At the early state, multiple nucleation events occur at the corners and sides of the confining hexagon. These domains then grow into the central region of the hexagon. The nonuniform advancing front of the domains implies that nucleations occur earlier at the corners than those at the sides, i.e. that the nucleation rate at the corners is higher than that at the sides. In contrast to the case of $\bar{\phi}_C = 0.100$, there is no spontaneous nucleation events observed in the central region. Thus, the ordered domains originated from the corners and sides continuously grow to fill the entire region of the confining hexagon, resulting in the completely phase-separated morphology shown in Figure 1b2. The Delaunay triangles shown in Figure 1b3 exhibit a small amount of defects, $f_{DF} \approx 0.70\%$. Obviously, the formation of these defects is from the grain boundaries between domains originated from the nucleation events occurring at the sides with random positions, because the positions of these domains are in general incommensurate with those ordered domains nucleated earlier at the corners. This observation implied that, in order to avoid the incoherence between these two types of nuclei, the side-induced nucleation event should be suppressed so that the ordering kinetics is dictated by the six coherent domains from the corner-induced nucleation. This can be achieved, as shown below, by reducing the concentration of the homopolymers further such that the side-induced nucleation is suppressed, whereas the disordered state is still kept as a metastable state.

The condition to suppress all nucleation events except for the corner-induced nucleation can be obtained by setting the homopolymers concentration at a value of $\bar{\phi}_C = 0.035$. The morphologies at this homopolymer concentration are plotted in Figure 1c. The structures at the early and late stages clearly demonstrate that the nucleation and growth of the ordered domains are dictated by the corner-induced nucleation. At the early stage as shown in Figure 1c1, there are six ordered domains originated from the six corners and these domains grow coherently toward the center of the system. At the late


DOI: 10.1021/acs.macromol.5b00681
*Macromolecules* 2015, 48, 4174−4182

stage there is no spontaneous nucleation occuring at the central region and, due to the commensurate position and orientation of the corner-induced nuclei, the six domains merge to form a perfectly ordered pattern filling up the entire region of the hexagon (Figure 1c3). These results demonstrate that the corners of the confining hexagon could act as nucleation agents with the highest nucleation rate as compared with the side-induced nucleation and spontaneous nucleation processes, thus verifying the prediction of the classical nucleation theory given in the SI.

It should be pointed out that the addition of homopolymers not only alters the phase separation kinetics but also impacts the growth speed of ordered domains in the disordered state. The growing speed can be quantified by the growing number of domains $n_{MD}$ as a function of time during the period of domain growth. The results of time evolution of $n_{MD}$ for various values of $\bar{\phi}_C$ and fixed $D = 41.00\ L_0$ are present in Figure 2a. Note that

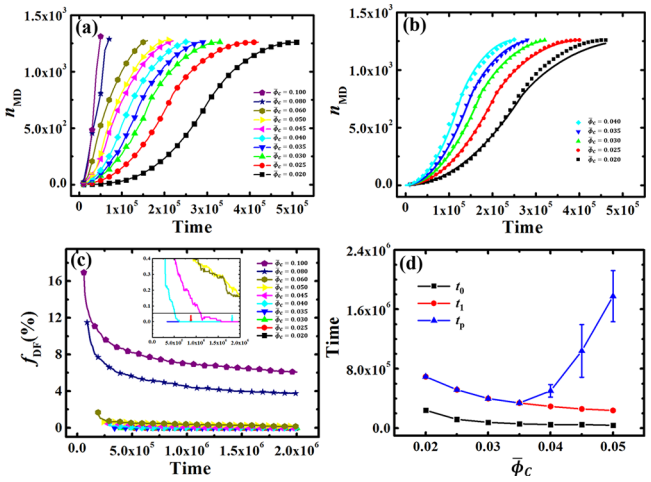


**Figure 2.** Time evolution of microdomain number ($n_{MD}$) (a) and its fitting graph (b), and defect concentration ($f_{DF}$) as a function of time (c) for various $\bar{\phi}_C$. (d) Incubation time ($t_0$), growth time ($t_1$) and ordering time ($t_p$) as a function of $\bar{\phi}_C$.

each set of the data presented in Figure 2a has been shifted by its corresponding incubation time, so that in the plot the domain growth of each sample starts at the same time. At high homopolymer concentrations $\bar{\phi}_C \geq 0.080$, homogeneous nucleation rate is so high that a spontaneous phase separation happens simultaneously in the central disordered area of the sample before the surface-induced nucleation domains grow up to occupy the entire sample. Accordingly, there is only a short period of time for the growth of the multiple nucleation domains. When the homopolymer concentration is intermediate between 0.045 and 0.080, the phase separation is governed by the surface-induced nucleation and growth process. Although the nucleation rate at the sides is intermediate between the spontaneous nucleation rate and the heterogeneous nucleation rate at the corners, it is still considerably high. Nucleation events are induced by the sidewalls at random locations along the sides and at unpredictable time soon after the induced nucleations by the corners and therefore make the advancing front of multiple domain grains more irregular. Nevertheless, the comparison of the domain growth between $\bar{\phi}_C = 0.060$, 0.050, and 0.045, indicates that higher homopolymer composition gives rise to faster domain growth, which is dictated by the stronger driving force of domain formation at the higher segregation degree caused by increased homopolymer composition. As $\bar{\phi}_C$ is reduced to be lower than 0.040, the nucleation rate at the sides is modified to be significantly lower than that at the corners, and consequently it is unable to lead to any nucleation occurrence during the growth period of the nucleation domains almost simultaneously induced by the six corners. The synchronic growth of the six domain grains enables one to predict the time evolution of domain number by simply assuming a space-independent moving line speed $v$ of the advancing front and dividing the growth period into two stages: individual growth stage in which each grain grows independently before they meet each other, and the overall growth stage in which six grains merge into each other to form a unified advancing front. The derived function measuring the time function of domain number in eq 6 fits the data of $0.020 \leq \bar{\phi}_C \leq 0.040$ well (Figure 2b), and the fitting gives rise to the line speed $v$ almost linearly dependent on the homopolymer composition.

$$n_{MD} = \begin{cases} 2\pi v^2 t^2 & t < \dfrac{D}{4v} \\ 6\left[\dfrac{D}{4}\left(v^2t^2 - \dfrac{D^2}{16}\right)^{1/2} + \left(\dfrac{\pi}{3} - \arccos\dfrac{D}{4vt}\right) v^2t^2\right] & t \geq \dfrac{D}{4v} \end{cases} \tag{6}$$

The kinetics of the ordering process can be quantified by one time scale, $t_1$, at which the growth of the ordered domains is completed such that the entire hexagon is filled with ordered domains. The ordering process after this time involves the elimination of defects in the system. The time evolution of average defect concentration (denoted as $f_{DF}$) starting from $t_1$ for various $\bar{\phi}_C$ is shown in Figure 2c. Each defect concentration is averaged on eight independent simulations with the same set of parameters but initialized with different random conditions. Apparently, for high homopolymer compositions $\bar{\phi}_C = 0.100$ and 0.080, the defect concentration at the beginning is very high, and it decreases fast at the initial stage in which isolated disclination and dislocation defects and small clusters of dislocations are being removed.[9,41,56] As the defect evolution becomes slower and slower, and the ordering time, $t_p$, moves toward the defect-free pattern with respect to the diagonal size, $D$ increases roughly according to a power law, $t_p \sim (D/L_0)^{1/\nu}$ ($\nu \approx 0.22$), for a typical spinodal-process formed domains, where the coefficient $\nu$ is dictated by the evolution behavior of the intrinsic correlation length in the hexagonal cylinders.[41] When the domain formation changes from mixed nucleation and spinodal process to a nucleation-dominated one by lowering the homopolymer concentration, the initial defect concentration decreases drastically, usually lower than 1% for $\bar{\phi}_C \leq 0.050$. Accordingly, the annihilation process of defects is speeded up, and it deviates from the power law of the ordering time in the spinodal case. Inset of Figure 2c implies that it is possible to remove all the defects in the samples of $\bar{\phi}_C = 0.050$ and 0.060 in a reasonable annealing time because the concentration of survived defects is already so low as 0.1–0.2% after $2 \times 10^6$ steps corresponding to one or two disclinations in the entire sample of $D = 41.00\ L_0$ (total 1261 domains are contained in the perfect pattern).[41] As the homopolymer composition is lowered further approaching to the case where the nucleation and growth process is dictated by


DOI: 10.1021/acs.macromol.5b00681
Macromolecules 2015, 48, 4174–4182

the corner-induced nucleation, the ordering process is usually finished in the cutoff time of $2 \times 10^6$ steps. Specifically, for $\bar{\phi}_C < 0.040$, the domains are indeed perfectly ordered as soon as the domain growth of the six corner-induced grains ends.

Three characteristic times of the pattern formation in the hexagonally confined AB/C blends, i.e., the incubation time $t_0$, the domain growth time $t_1$, and the ordering time of patterns $t_p$, are estimated by averaging on eight independent runs of each system in our simulations for the range of $\bar{\phi}_C$ leading to nucleation-dominated formation of domains (Figure 2d). Importantly, increasing the homopolymer concentration drives the phase separation moving far away from the ideal coherent nucleation and growth process and hence raises the ordering time drastically, even though the incubation time and growth time at large $\bar{\phi}_C$ are shortened accordingly. Even for $\bar{\phi}_C = 0.020$, the incubation time is still acceptable, and moreover, the incubation time can be shortened by increasing the directing ability of the nucleation agent, e.g., strengthening the surface interactions of the sidewalls. From these discussions we can conclude that the window of homopolymer concentration of $0.020 \leq \bar{\phi}_C < 0.040$ is ideally suitable for the fabrication of perfectly ordered hexagonal patterns via DSA on topographically hexagonal templates.

**Effects of External Field.** Besides the homopolymer concentration, the strength of the interaction field between the polymers and the sidewalls is another critical factor impacting the self-assembly of block copolymers confined in the hexagonal wells, in particular, the nucleation rate near the walls. In contrast to the effect of the homopolymer concentration which regulating the phase behavior of the bulk system, the surface field is a short-ranged directing field which only has a local effect on the pattern formation. In fact, one of the most important roles of the surface field is to serve as nucleation agents directing heterogeneous nucleation events at the six corners. In order to achieve this goal, the surface field has to be optimized so that it can induce nucleation events at the corners while suppress the nucleation at the sidewalls, thereby inducing coherent nucleation exclusively at the six corners.

We investigate the effects of the field strength on the ordering kinetics of the confined blends with a fixed commensurate size $D = 41.00\ L_0$ and $\bar{\phi}_C = 0.035$. This set of parameters allows spontaneous nucleation in the bulk but with a sufficiently low nucleation rate. Such low homogeneous nucleation rate enables us to focus on the induced nucleation by the sides or the corners without any spontaneous nucleation. Morphologies at two times for three typical field strengths, $\Lambda_0 = 0.0080$, 0.0028, and 0.0020, are present in Figure 3. For $\bar{\phi}_C = 0.035$, a strong surface field with $\Lambda_0 = 0.0080$ induces multiple nucleation events at the corners as well as at the sides (Figure 3a), which is similar as the sample with a higher composition $\bar{\phi}_C = 0.050$ but a lower field strength $\Lambda_0 = 0.0020$ in Figure 1b. This indicates that both the homopolymer composition and the surface field can modify the nucleation rate, but through different mechanisms. The homopolymers concentration modifies the homogeneous nucleation rate, whereas the interaction strength determines the rate of heterogeneous nucleation at the sides and corners.

When the field strength is decreased to be $\Lambda_0 = 0.0028$ (Figure 3b), we find that there are six synchronic nuclei at the early stage, $t = 8 \times 10^4$. However, it is surprising to observe that additional nucleation is induced by the sides at the region between two adjacent corners during the period of domain growth. As a result, the growth of the additional nuclei with incommensurate positions to those corner-induced nuclei leads to the formation of defects at the grain boundaries between the different domains (Figure 3b3). This observation implies that the heterogeneous nucleation rate directed by the sides is still too high as compared with the rate of the corner-induced nucleation. In other words, the difference of the incubation times between these two types of heterogeneous nucleation events is not large enough, so that the growth of the corner-induced domains is interrupted by the side-induced domains. In order to suppress the side-induced nucleation, the surface field should be weakened further. Of course, decreased strength of the surface field can lower the rate of corner-induced and side-induced nucleations simultaneously. Therefore, decreasing the interaction strength does not guarantee the exclusive occurrence of corner-induced nucleations. On the other hand, it is possible to increase the difference of the incubation times between the two induced nucleation events because the incubation time depends sensitively on the nucleation rate or the energy barrier. From the simulations, it is seen that when the field strength is slightly reduced to be $\Lambda_0 = 0.0020$, coherent nuclei are induced synchronically at the six corners and their growth proceeds without the intervention from any side-induced nucleation, leading to the formation of defect-free hexagonal patterns in the hexagonal well (Figure 3c).

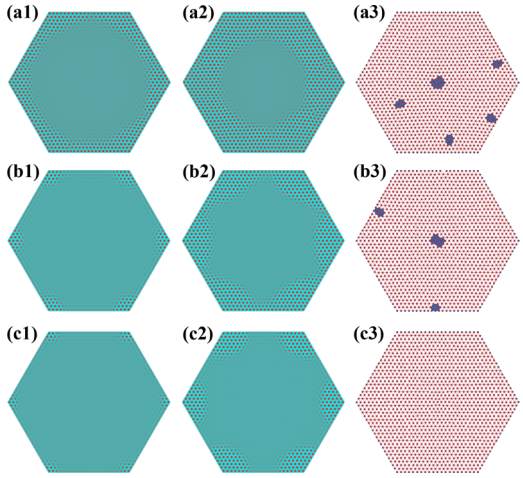


**Figure 3.** Morphology snapshots (left and middle) and the corresponding Delaunay Triangle plots (right column) at two times $t = 8 \times 10^4$ and $14 \times 10^4$ for three typical field strengths: (a) $\Lambda_0 = 0.0080$; (b) $\Lambda_0 = 0.0028$; (c) $\Lambda_0 = 0.0020$. The size of hexagon and homopolymer concentration are fixed as $D = 41.00\ L_0$ and $\bar{\phi}_C = 0.035$, respectively.

**Size Effect and Size Commensurability Window of the Hexagons.** Intuitively, the positional commensurability of the six nucleated nuclei is dictated by the size of the hexagon. In particular, commensurability is achieved when the diagonal size of hexagon $D$ is an odd integer multiples of the domain spacing $L_0$. The hexagons with commensurate sizes can therefore be quantified by an odd integer $m$ which is defined as the ratio between the size of hexagon and the domain period, $m = D/L_0$. In principle, the ordering process of the cylinder patterns governed by the coherent corner-induced nuclei and their growth should be independent of the commensurate value of $m$; i.e., perfectly ordered patterns should be obtained as long as $m$ is an odder integer. We have verified this simple prediction by simulating the systems of fixed $\bar{\phi}_C = 0.035$ and $\Lambda_0 = 0.0020$ with a series of values, $m = 21$, 31, 41, 51, and 61. The desired


DOI: 10.1021/acs.macromol.5b00681
Macromolecules 2015, 48, 4174−4182

corner-induced coherent nucleation and growth process is observed in each system, resulting in the formation of defect-free pattern. We have tested the limit of this strategy by increasing $m$ to 71, and we observed additional side-induced nucleation at random positions between two adjacent corners during the prolonged growth period of the corner-induced domains in such large hexagon. The presence of these incoherently nucleated the domains disrupts the epitaxial growth of the six coherent domains, resulting in the introduction of defects to the system within the characteristic time of $t_1$. It is worth to notice that the side-induced domains usually lead to the formation of defected patterns with a low defect density, therefore the defects could be removed within a reasonable annealing time. On one hand, the imperfection becomes more severe as the hexagonal size is increased because more side-induced nucleation events can potentially occur in a larger hexagon. Of course the rate of the side-induced nucleation could be lowered by changing the homopolymers concentration and/or the interaction strength. Furthermore, a more efficient, albeit more complex, strategy is to modify the sidewalls of the hexagon so that the corners are more attractive to the majority blocks of the diblock copolymer. Our simulations have demonstrated that this new patterning scheme based on specially engineered corners could be used to fabricate defect-free hexagonal patterns in macroscopically large hexagons, e.g., with such a large diagonal size of $D > 61\ L_0$, containing more than 2791 cylinder domains.

When the hexagonal size deviates from the commensurate condition of $mL_0$, where $m$ is an odd integer number, there is an increased possibility of defect formation because of the expansion or compression stresses induced by the incommensurability. In practice, one critical step of the strategy is to precisely manufacture the hexagonal wells with a controllable size according to the measured domain spacing of the prepared block copolymer/homopolymer blends in advance. Small degree of incommensurability is likely to be introduced in this procedure because of possible errors arising from the nanomanufacturing of the hexagons or from the measurement of the domain spacing. Therefore, it is crucial for the patterning method to have a certain degree of tolerance for the size incommensurability. We have examined the ordering process of the pattern formation in hexagons with sizes centered around a number of typical commensurate sizes $D = 21\ L_0$, $31\ L_0$, $41\ L_0$, and $51\ L_0$, in the range of $\delta D$ ($-L_0 < \delta D < L_0$), and then estimated the size commensurability window of forming defect-free patterns by tracing the defect evolution within a reasonable cutoff of annealing time, $2 \times 10^6$ steps, that corresponds to a real annealing time from hours to days depending on specific molecular weights.[41] In Figure 4a, it can be seen that the commensurability window is significantly wide for $21 \leq m \leq 51$ though it becomes narrow as the hexagonal size increases. For example, for $m = 51$, the commensurability window is $51L_0 \lesssim D \lesssim 51.4L_0$ with a width $0.4L_0$, about 8−10 nm, which is acceptable in modern lithography techniques. Figure 4b suggests that the ordering time is prolonged drastically when the hexagonal size deviates from the center of the commensurability window, and it becomes more disastrous for larger systems. Another noticeable interesting point is the asymmetry of the commensurability window that implies the asymmetric tolerance of the system to the domain expansion and compression, which is similar as that in the self-assembly of lamella-forming block copolymers on patterned surfaces.[57,58]

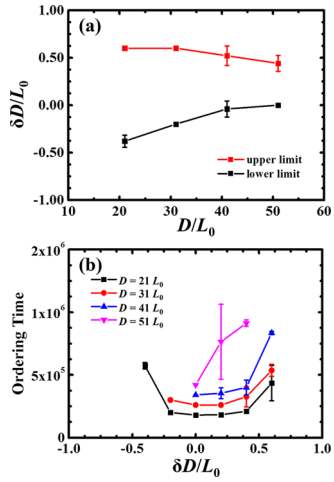


**Figure 4.** (a) Size commensurability windows for various sizes of hexagons, $m = D/L_0$. (b) Ordering time with respect to the size deviation $\delta D$. The field strength and homopolymer concentration are fixed as $\bar{\phi}_C = 0.035$ and $\Lambda_0 = 0.0020$, respectively.

## CONCLUSIONS

In summary, a high-efficient patterning method utilizing corner-induced heterogeneous nucleation of ordered domains from the six corners of directing hexagonal potential wells is proposed and demonstrated by simulations of the self-assembly of block copolymer/homopolymer blends confined in hexagonal wells. This method involves not only the control of the intrinsic phase-separation kinetics of the blends but also the regulation of the difference between the heterogeneous nucleation rate induced by the sides and that induced by the corners. There are three controllable variables to be optimized. First of all, the homopolymer composition is varied to tune the metastability of the disordered phase so that spontaneous nucleation of the disordered phase is suppressed. Then the interaction between the polymers and the confining sidewalls is tailored to control the surface-induced nucleation rate such that the nucleation events are induced exclusively by the six corners, leading to the formation of six nuclei of the ordered phase with controlled positions and orientations. The subsequent coherent growth of these six domains leads to the formation of defect-free patterns when the hexagonal size, as the third controlling parameter, is commensurate with the period of the ordered phase. The mechanism and validity of this method are demonstrated by the large-scale two-dimensional simulations. With a set of optimized parameters, defect-free hexagonal patterns in hexagons with the diagonal size as large as $D = 61L_0$ are achieved. Furthermore, an examination of size commensurability windows reveals the robustness of the proposed method.

The most challenging step in the proposed method is to control the surface interaction of the sidewalls. At the present time, standard surface-functionalization techniques have been developed to tune the surface affinity, e.g., polarization[13] and grafting random copolymer[59] or homopolymer brushes.[60] Some techniques have the capability to modify the surface interactions in a systematic manner, by controlling the exposure time of polarization[13] or the component of random copolymer brushes.[60,61] Specifically, the research group of Ross have demonstrated a surface modification scheme for topographically templates in which the floor surface and the sidewall surface are separately functionalized to be neutral and preferential, respectively.[62] Their method provides an ideal


DOI: 10.1021/acs.macromol.5b00681
Macromolecules 2015, 48, 4174−4182

candidate for the surface functionalization of the hexagonal wells in this work. In addition, if an additional measure (e.g., locally atomic force microscopic etching) for improvement is introduced to change the homogeneous surface potential of the sidewalls to be inhomogeneous, i.e., specially stronger at the six corners that further enlarges the induced nucleation rate at the corners relative to that at the sides, the regulation difficulty of the difference of the nucleation rates could be eliminated and therefore defect-free patterns could be achieved in larger systems. For example, in Figure 5, we observe defect-free

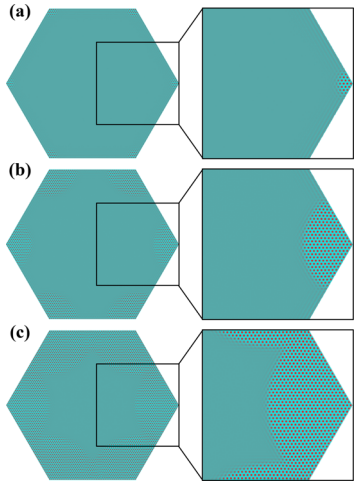


**Figure 5.** Morphology snapshots indicating the formation of defect-free pattern in an extremely large hexagon, $D/L_0 = 91$, in which the surface strength is specially strengthened at the corners: (a) $t = 10 \times 10^4$, (b) $t = 25 \times 10^4$, and (c) $t = 40 \times 10^4$.

patterns in the hexagon with $D = 91L_0$ by increasing the surface strength locally at the corners. In principle, this patterning technique combined with this improvement does not exhibit a size limit except for the intervention of possible spontaneous nucleations in the bulk during a long domain growth time when the hexagon becomes extraordinary large.

Although our simulations are mainly conducted in two dimensions, the conclusions from our study are valid for the thin film systems of finite thickness and of a bulk equilibrium ordered phase as hexagonal cylinder instead of sphere (see the movie clip in SI).[34] The DSA strategy demonstrated in this study is independent of the specific model in that the specific conditions of obtaining defect-free patterns using DSA of block copolymers apply to any systems exhibiting phase transition kinetics. In addition, the fundamental idea can be extended to the order−order transition in which the stable ordered phase nucleates from another metastable ordered phase for the fabrication of defect-free domain patterns.

## ■ ASSOCIATED CONTENT

### Supporting Information

Tolerance for angular deviation, classical nucleation theory of homo/heterogeneous nucleation, and a video clip of a 3-D simulation sample. The Supporting Information is available free of charge on the ACS Publications website at DOI: 10.1021/acs.macromol.5b00681.

## ■ AUTHOR INFORMATION

### Corresponding Author

*(W.L.) E-mail: weihuali@fudan.edu.cn. Telephone: +86 (0)21 65643579. Fax: +86 (0)21 65640293.

### Notes

The authors declare no competing financial interest.

## ■ ACKNOWLEDGMENTS

The authors thank R. A. Wickham for constructive comments and helpful discussions. The authors thank the funding support by the National Natural Science Foundation of China (NSFC) (Grants Nos. 21322407 and 21174031). A.-C.S. acknowledges the support from the Natural Science and Engineering Research Council (NSERC) of Canada.

## ■ REFERENCES

(1) Moore, G. E. *Proc. IEEE* **1998**, *86*, 82−85.
(2) Gelsinger, P. *Solid-State Circuits Newsl., IEEE* **2006**, *11*, 18−20.
(3) Mansky, P.; Haikin, P.; Thomas, E. L. *J. Mater. Sci.* **1995**, *30*, 1987−1992.
(4) Bang, J.; Jeong, U.; Ryu, D. Y.; Russell, T. P.; Hawker, C. J. *Adv. Mater.* **2009**, *21*, 4769−4792.
(5) Jung, Y. S.; Chang, J. B.; Verploegen, E.; Berggren, K. K.; Ross, C. A. *Nano Lett.* **2010**, *10*, 1000−1005.
(6) Carter, K. R. *ACS Nano* **2010**, *4*, 595−598.
(7) Griffiths, R. A.; Williams, A.; Oakland, C.; Roberts, J.; Vijayaraghavan, A.; Thomson, T. *J. Phys. D: Appl. Phys.* **2013**, *46*, 503001.
(8) Ruiz, R.; Kang, H. M.; Detcheverry, F. A.; Dobisz, E.; Kercher, D. S.; Albrecht, T. R.; de Pablo, J. J.; Nealey, P. F. *Science* **2008**, *321*, 936−939.
(9) Li, W. H.; Qiu, F.; Yang, Y. L.; Shi, A. C. *Macromolecules* **2010**, *43*, 1644−1650.
(10) Li, W. H.; Xie, N.; Qiu, F.; Yang, Y. L.; Shi, A. C. *J. Chem. Phys.* **2011**, *134*, 144901.
(11) Tang, Q. Y.; Ma, Y. Q. *Soft Matter* **2010**, *6*, 4460−4465.
(12) Chakrabarti, A.; Chen, H. *J. Polym. Sci., Part B: Polym. Phys.* **1998**, *36*, 3127−3136.
(13) Kim, S. O.; Solak, H. H.; Stoykovich, M. P.; Ferrier, N. J.; de Pablo, J. J.; Nealey, P. F. *Nature* **2003**, *424*, 411−414.
(14) Park, S. M.; Stoykovich, M. P.; Ruiz, R.; Zhang, Y.; Black, C. T.; Nealey, P. F. *Adv. Mater.* **2007**, *19*, 607−611.
(15) Cheng, J. Y.; Rettner, C. T.; Sanders, D. P.; Kim, H. C.; Hinsberg, W. D. *Adv. Mater.* **2008**, *20*, 3155−3158.
(16) Park, S. M.; Rettner, C. T.; Pitera, J. W.; Kim, H. C. *Macromolecules* **2009**, *42*, 5895−5899.
(17) Liu, G. L.; Detcheverry, F.; Ramirez-Hernandez, A.; Yoshida, H.; Tada, Y.; de Pablo, J. J.; Nealey, P. F. *Macromolecules* **2012**, *45*, 3986−3992.
(18) Perera, G. M.; Wang, C. Q.; Doxastakis, M.; Kline, R. J.; Wu, W. L.; Bosse, A. W.; Stein, G. E. *ACS Macro Lett.* **2012**, *1*, 1244−1248.
(19) Segalman, R. A.; Yokoyama, H.; Kramer, E. J. *Adv. Mater.* **2001**, *13*, 1152−1155.
(20) Segalman, R. A.; Hexemer, A.; Kramer, E. J. *Macromolecules* **2003**, *36*, 6831−6839.
(21) Park, O. H.; Cheng, J. Y.; Hart, M. W.; Topuria, T.; Rice, P. M.; Krupp, L. E.; Miller, R. D.; Ito, H.; Kim, H. C. *Adv. Mater.* **2008**, *20*, 738−742.
(22) Yang, J. K. W.; Jung, Y. S.; Chang, J. B.; Mickiewicz, R. A.; Alexander-Katz, A.; Ross, C. A.; Berggren, K. K. *Nat. Nanotechnol.* **2010**, *5*, 256−260.
(23) Chang, J. B.; Son, J. G.; Hannon, A. F.; Alexander-Katz, A.; Ross, C. A.; Berggren, K. K. *ACS Nano* **2012**, *6*, 2071−2077.
(24) Mishra, V.; Fredrickson, G. H.; Kramer, E. J. *ACS Nano* **2012**, *6*, 2629−2641.
(25) Hannon, A. F.; Gotrik, K. W.; Ross, C. A.; Alexander-Katz, A. *ACS Macro Lett.* **2013**, 251−255.



DOI: 10.1021/acs.macromol.5b00681
*Macromolecules* 2015, 48, 4174−4182

(26) Zhang, L. S.; Wang, L. Q.; Lin, J. P. *ACS Macro Lett.* **2014**, *3*, 712−716.
(27) Stoykovich, M. P.; Müller, M.; Kim, S. O.; Solak, H. H.; Edwards, E. W.; de Pablo, J. J.; Nealey, P. F. *Science* **2005**, *308*, 1442−1446.
(28) Stoykovich, M. P.; Kang, H. M.; Daoulas, K. C.; Liu, G. L.; Liu, C. C.; de Pablo, J. J.; Müller, M.; Nealey, P. F. *ACS Nano* **2007**, *1*, 168−175.
(29) Chang, J. B.; Choi, H. K.; Hannon, A. F.; Alexander-Katz, A.; Ross, C. A.; Berggren, K. K. *Nat. Commun.* **2014**, *5*, 9.
(30) Hashimoto, T.; Sakamoto, N. *Macromolecules* **1995**, *28*, 4779−4781.
(31) Hashimoto, T.; Sakamoto, N.; Koga, T. *Phys. Rev. E* **1996**, *54*, 5832−5835.
(32) Vega, D. A.; Gomez, L. R. *Phys. Rev. E* **2009**, *79*, 051607.
(33) Pezzutti, A. D.; Vega, D. A. *Phys. Rev. E* **2009**, *84*, 051607.
(34) Xie, N.; Li, W. H.; Qiu, F.; Shi, A. C. *Soft Matter* **2013**, *9*, 536−542.
(35) Chen, P.; Liang, H. J.; Shi, A. C. *Macromolecules* **2007**, *40*, 7329−7335.
(36) Yu, B.; Sun, P. C.; Chen, T. H.; Jin, Q. H.; Ding, D. T.; Li, B. H.; Shi, A. C. *Phys. Rev. Lett.* **2006**, *96*, 138306.
(37) Yu, B.; Jin, Q. H.; Ding, D. T.; Li, B. H.; Shi, A. C. *Macromolecules* **2008**, *41*, 4042−4054.
(38) Wu, Y. Y.; Cheng, G. S.; Katsov, K.; Sides, S. W.; Wang, J. F.; Tang, J.; Fredrickson, G. H.; Moskovits, M.; Stucky, G. D. *Nat. Mater.* **2004**, *3*, 816−822.
(39) Shin, K.; Xiang, H. Q.; Moon, S. I.; Kim, T.; McCarthy, T. J.; Russell, T. P. *Science* **2004**, *306*, 76.
(40) Tang, C. B.; Bang, J.; Stein, G. E.; Fredrickson, G. H.; Hawker, C. J.; Kramer, E. J.; Sprung, M.; Wang, J. *Macromolecules* **2008**, *41*, 4328−4339.
(41) Xu, Y. C.; Xie, N.; Li, W. H.; Qiu, F.; Shi, A. C. *J. Chem. Phys.* **2012**, *137*, 194905.
(42) Hardy, C. G.; Tang, C. B. *J. Polym. Sci., Part B: Polym. Phys.* **2013**, *51*, 2−15.
(43) Xu, J.; Park, S.; Wang, S.; Russell, T. P.; Ocko, B. M.; Checco, A. *Adv. Mater.* **2010**, *22*, 2268−2272.
(44) Spencer, R. K. W.; Wickham, R. A. *Soft Matter* **2013**, *9*, 3373−3382.
(45) Qin, J.; Khaira, G. S.; Su, Y. R.; Garner, G. P.; Miskin, M.; Jaeger, H. M.; de Pablo, J. J. *Soft Matter* **2013**, *9*, 11467−11472.
(46) Ohta, T.; Ito, A. *Phys. Rev. E* **1995**, *52*, 5250−5260.
(47) Ito, A. *Phys. Rev. E* **1998**, *58*, 6158−6165.
(48) Oono, Y.; Puri, S. *Phys. Rev. Lett.* **1987**, *58*, 836−839.
(49) Oono, Y.; Puri, S. *Phys. Rev. A* **1988**, *38*, 434−453.
(50) Puri, S.; Oono, Y. *Phys. Rev. A* **1988**, *38*, 1542−1565.
(51) Fredrickson, G. H. *The Equilibrium Theory of Inhomogeneous Polymers*; Clarendon Press: Oxford, U.K., 2006.
(52) Shi, A. C. In *Self-consistent field theory of block copolymers*; Hamley, I., Ed.; Developments in Block Copolymer Science and Technology; Wiley: New York, 2004; pp 265−293.
(53) Yeung, C.; Shi, A. C. *Macromolecules* **1999**, *32*, 3637−3642.
(54) Ohta, T.; Kawasaki, K. *Macromolecules* **1986**, *19*, 2621−2632.
(55) Hur, S. M.; Garcia-Cervera, C. J.; Kramer, E. J.; Fredrickson, G. H. *Macromolecules* **2009**, *42*, 5861−5872.
(56) Vega, D. A.; Harrison, C. K.; Angelescu, D. E.; Trawick, M. L.; Huse, D. A.; Chaikin, P. M.; Register, R. A. *Phys. Rev. E* **2005**, *71*, 12.
(57) Nagpal, U.; Müller, M.; Nealey, P. F.; de Pablo, J. J. *ACS Macro Lett.* **2012**, *1*, 418−422.
(58) Xie, N.; Li, W. H.; Zhang, H. D.; Qiu, F.; Shi, A. C. *J. Chem. Phys.* **2013**, *139*, 9.
(59) Mansky, P.; Russell, T. P.; Hawker, C. J.; Mays, J.; Cook, D. C.; Satija, S. K. *Phys. Rev. Lett.* **1997**, *79*, 237−240.
(60) Edwards, E. W.; Montague, M. F.; Solak, H. H.; Hawker, C. J.; Nealey, P. F. *Adv. Mater.* **2004**, *16*, 1315−1319.
(61) Liu, C. C.; Ramirez-Hernandez, A.; Han, E.; Craig, G. S. W.; Tada, Y.; Yoshida, H.; Kang, H.; Ji, S.; Gopalan, P.; de Pablo, J. J.; Nealey, P. F. *Macromolecules* **2013**, *46*, 1415−1424.
(62) Son, J. G.; Gwyther, J.; Chang, J.-B.; Berggren, K. K.; Manners, I.; Ross, C. A. *Nano Lett.* **2011**, *11*, 2849−2855.


DOI: 10.1021/acs.macromol.5b00681
*Macromolecules* 2015, 48, 4174−4182